Green Chemistry

RSC Publishing

PAPER

View Article Online
View Journal | View Issue

Cite this: *Green Chem.*, 2013, **15**, 3057

Self-assembly of NiO nanoparticles in lignin-derived mesoporous carbons for supercapacitor applications†

Feng Chen, Wenjing Zhou, Hongfei Yao, Ping Fan, Jintao Yang,* Zhengdong Fei and Mingqiang Zhong*

We demonstrate the self-assembly of highly dispersed NiO nanoparticles embedded in lignin-derived mesoporous carbon (MPC) frameworks. Self-assembly is induced by evaporation of the solvent from a mixture of metal-containing liquid crystalline mesophases of lignin-derived polymers and transition metal nitrate hydrate, which yielded NiO@MPC nanostructures at 600 °C under a N_2 atmosphere. The microstructure and morphology of the NiO@MPC are characterized by XRD, TEM and BET. The results show that the NiO nanoparticles are highly dispersed in a mesoporous carbon matrix. The NiO@MPC composites show metal oxide contents in the range 49–79 wt%, high surface areas (503–802 $m^2\ g^{-1}$), uniform pore sizes (≈3.7 nm), various porous distributions and large pore volumes (0.46–0.68 $cm^3\ g^{-1}$). Electrochemical studies were carried out by measurement of cyclic voltammetry (CV) and charge–discharge tests. The results demonstrate that the NiO@MPC composites have high specific capacitance (880.2 F g^{-1} at a current density of 1.0 A g^{-1}) and display good retention. 90.9% of the specific capacitance is retained when the current density changes from 1 A g^{-1} to 10 A g^{-1} in the charge–discharge tests and 93.7% of the specific capacitance is retained after 1000 charge–discharge cycles. Thus, the NiO@MPC composites are promising supercapacitor electrode materials.

Received 7th June 2013,
Accepted 12th August 2013

DOI: 10.1039/c3gc41080c

www.rsc.org/greenchem

Introduction

Supercapacitors have attracted much attention in recent years as they have the potential to satisfy the demand for both huge energy and power density in many advanced technologies.[1,2] However, their poor conductivity and cycling stability remain the major obstacles for their widespread application. Many materials have been investigated as the electrode materials in supercapacitors, including transition metal oxides,[3,4] carbonaceous materials[5,6] and conducting polymers.[7,8] Among them, NiO has been considered as one of the most promising electrode materials due to its good pseudo-capacitive behaviour, low cost, environmental benignity and practical availability.[9,10] However, like other transition metal oxide materials, the poor conductivity, cycling stability and rate capability of NiO have limited its high specific capacitance potential in practical applications. On the other hand, carbon materials have high power density and long cycle life; nevertheless, the low specific capacitance greatly limits their further application. Therefore, this has inspired attempts to develop novel electrode materials *via* the coupling of NiO and carbon materials as electrodes for supercapacitors.

The metal oxide@carbon composites not only increase the utilization of the active materials, but also improve the electrical conductivity and mechanical strength of the composite materials. In this approach, it is essential to load and/or incorporate metal oxide nanoparticles into the nanostructured carbon materials, which can be carbon nanotubes,[11] carbon aerogels,[12] mesoporous carbons (MPCs),[13] graphene,[14] *etc.* A recent report shows that reduced graphene oxide (RGO) and $Ni(OH)_2$ composite films synthesized by electrophoretic deposition have an excellent specific capacitance of 1404 F g^{-1} at 2 A g^{-1}.[15] However, there are few reports on the synthesis of rational core–shell structures consisting of MPC shells located outside and NiO embedded inside. Li *et al.* have reported peapod-like Ni@MPC core–shell nanowires,[16] in which electrochemical oxidation of nano-sized Ni to its corresponding NiO could be carried out. The composite electrode exhibited higher specific capacitance with enhanced rate capability and cycling stability in 1 M KOH aqueous solution. However, the expensive dopamine was selected as the carbon precursor. Wan *et al.* have also reported the self-assembly of Ni and NiO

College of Materials Science and Engineering, Zhejiang University of Technology, Hangzhou, 310014, China. E-mail: yangjt78@hotmail.com, zhongmq@zjut.edu.cn; Fax: +86-571-88320856; Tel: +86-571-88320856

†Electronic supplementary information (ESI) available: The EDX figure of G-NiO@C-1 sample; the TEM image of higher NiO-containing samples; the electrochemical property figures of G-NiO@C-3 and F-NiO@C-3. See DOI: 10.1039/c3gc41080c

nanoparticles embedded in ordered MPC and polymer frameworks.[17] The mesoporous solids show excellent adsorption properties for dyes and permit an easy magnetic separation procedure. This method is expected to be applicable to synthesis of supercapacitor materials. Nevertheless, there still exist several major drawbacks for NiO@carbon nanocomposite materials, such as their relatively low weight fraction of NiO.

Recently, the liquid-crystalline (LC) phase-templating method has offered an effective route for synthesizing MPCs.[18,19] The self-assembly of a mesostructure from a non-ionic surfactant and a carbon precursor is induced by solvent evaporation. MPCs with diverse mesostructures, pore sizes, and morphologies have been fabricated.[20–22] Non-metals and metal compounds can also be introduced into carbon pore walls during self-assembly. For fabrication of MPC structures, major advances have been made simultaneously by Zhao's and Dai's groups using all commercially available, low-cost phenolic resin materials.[23] For the fast development of LC phase-templating synthesis of MPCs, the exploration of their applications as electrochemical capacitors has been gradually carried out.

Lignin is a natural amorphous polymer in plants, which is composed of phenyl propane units substituted with one or two methoxyl groups. It is generally obtained, as a by-product in paper production, through separation from cellulose fibers by means of the pulping process, which presents environmental problems and gives altered lignin.[24] Considering this abundance of lignin, its chemical composition, and its functional characteristics in plants, it appears reasonable to examine the contribution that lignin can make as a substitute for phenolic resins.[25]

In this work, we have tried to obtain NiO@MPC composites with enhanced electrochemical characteristics using well known LC phase-templating preparation procedures with precisely selected carbonization for natural, plant-derived lignin precursors. The formaldehyde and glutaraldehyde were selected as cross-linking agents (CLAs). The resulting NiO@MPC materials show metal oxide contents in the range 49–79 wt%, high surface areas (503–802 $m^2\ g^{-1}$), uniform pore sizes (≈3.7 nm), various porous distributions and large pore volumes (0.46–0.68 $cm^3\ g^{-1}$).

The unique structure, when applied as a supercapacitor electrode, possesses three obvious advantages.[26,27] (a) The carbon layer coated on the surface of the NiO nanoparticles overcomes the poor conductivity of metal oxide. (b) The outer mesoporous carbon shells not only construct the conducting pathway for the system's electron transfer but also prevent the inner nanoparticles from aggregation and pulverization. (c) The mesoporous feature of the carbon shell not only ensures interaction between the electrolyte and the active inner materials, but also digests the possible volume changes while cycling. More significantly, we found that the present NiO@MPC electrode exhibited higher specific capacitance with enhanced rate capability and cycle stability in 6 M KOH aqueous solution.

Experimental

Chemicals

Poly(ethylene oxide)-*b*-poly(propylene oxide)-*b*-poly(ethylene oxide) triblock copolymers Pluronic F127 ($EO_{106}PO_{70}EO_{106}$, Mw = 12 600) and sodium lignosulphonate were purchased from Sigma-Aldrich Inc. Formalin solution (HCHO, 37.0–40.0 wt%), glutaraldehyde solution ($C_5H_8O_2$, 50 wt%), potassium hydroxide (KOH, minimum 98.0%), ethanol (C_2H_5OH, minimum 99.7 wt%), and nickel nitrate ($Ni(NO_3)_2\cdot 6H_2O$, 98.0 wt%) were purchased from Aladdin Chemical Reagent Inc. All reagents were used as received without any further purification. Deionized water was used throughout the experiment.

Preparation of NiO@MPCs

In a typical synthesis, 0.5 g $Ni(NO_3)_2\cdot 6H_2O$ and 0.5 g Pluronic F127 were dissolved in ethanol (10.0 g), then 1.0 g sodium lignosulfonate was added to the above solution. After that, the formalin solution 2.0 g (containing 0.67 g formaldehyde) and 1.0 g KOH were slowly added sequentially under continuous magnetic stirring. The mixture sol was poured into Petri dishes to evaporate the ethanol and water at room temperature. Then the dishes were placed in an oven (80 °C) for 8 h to complete polymerization. The powders were scraped from the dishes for further heat treatment in a tubular furnace under the protection of a nitrogen atmosphere.

The temperature program involved heating from ambient temperature to 600 °C at a ramp rate of 5 °C min^{-1}. Finally, the resulting products were carbonized and reduced to the NiO@MPCs in flowing nitrogen at 600 °C for 2 h.

The sample was named F-NiO@C-1 (the first alphabet in the name denotes the CLA of formaldehyde, G represents the CLA of glutaraldehyde, and the last number denotes the weight ratio of Ni/lignin in the initial solution). In the different batches, we fixed the mass amounts of lignin and Pluronic P123, and adjusted the amount of $Ni(NO_3)_2\cdot 6H_2O$ in the range 0.5–2.5 g to tune the NiO contents in the final products.

Sample characterization

The X-ray diffraction (XRD) data were recorded on a Thermo Arl Scintag Xtra apparatus using Cu Kα radiation (k = 1.54056 Å) operated at 45 kV, 40 mA and a speed of 2° min^{-1} at room temperature. N_2 adsorption–desorption isotherms were recorded using the automatic volumetric sorption analyzer Micromeritics ASAP 2020 at 77 K (liquid nitrogen cooled). High-resolution transmittance electron microscopy (HRTEM) analysis was performed using a 300 kV JEM-100 CX II transmittance electron microscope. TEM samples were prepared by dispersing a small amount of sample in ethanol and subsequently depositing onto copper grids. Scanning electron micrographs (SEM, Hitachi S-4700) were taken to analyze the morphologies of the materials. The samples were previously coated with platinum. The Ni contents of the resulting samples were calculated by energy dispersive X-ray spectroscopy (EDX) analysis.

Electrode preparation

The electrode of NiO@MPC was prepared according to the following steps. 80 wt% NiO@MPC, 10 wt% acetylene black and 10 wt% polyvinylidene fluoride (PVDF) were well mixed to yield a paste. *N*-Methyl-2-pyrrolidone (NMP) was used as a solvent. Then the obtained paste was pressed onto nickel foam (1.2×10^7 Pa) that serves as a current collector (surface area is 1 cm^2). The prepared working electrodes were dried at room temperature for 1 day, and then under vacuum at room temperature overnight.

Electrochemical tests

Electrochemical studies were carried out by measurement of cyclic voltammetry (CV), electrochemical impedance and charge–discharge tests. The electrolyte used was 6 M KOH solution. A beaker type three-electrode cell equipped with a sample current collector on nickel foam as a working electrode, an Ag/AgCl electrode as a reference electrode, and a Pt plate (1 cm × 1 cm) as a counter electrode was used. A Luggin capillary tip was kept as close as 1–2 mm to the working electrode, and was set to minimize error due to iR drop in the electrolyte.

In comparison, a galvanostatic constant-current charge–discharge test was performed for measuring the specific capacitances (C_s) that are calculated from the first discharge curves using the following eqn (1):

$$C_s = I\Delta t/m\Delta V \quad (1)$$

where C_s (F g^{-1}) is specific capacitance, I (A) represents the current applied and m (g), ΔV (V) and Δt (s) designate the mass of the active materials, potential drop during discharge and total discharge time, respectively.

Results and discussion

NiO@MPCs were mainly synthesized by the *in situ* carbonization of nickel salt and carbon composites under a nitrogen atmosphere. The major process steps employed in this work are illustrated in Scheme 1. Briefly, nickel salt was firstly dissolved in Pluronic F127. Then LC phases containing F127 and nickel salt were self-assembled with the carbon precursors of lignosulfonate and different CLAs. After that, pre-polymerization of the lignin precursor and *in situ* deposition of the nickel salt were induced, sequentially. Finally, the nickel salt and carbon composites were calcinated at 600 °C under the protection of a nitrogen atmosphere, and NiO@MPCs could be obtained.

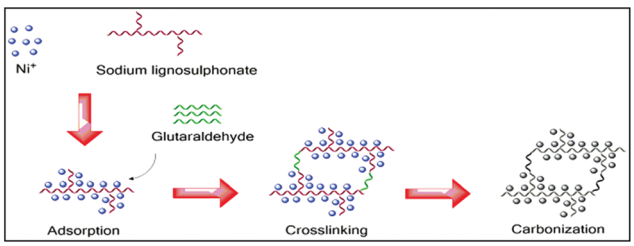

Scheme 1 The growth mechanism for NiO@MPC samples.

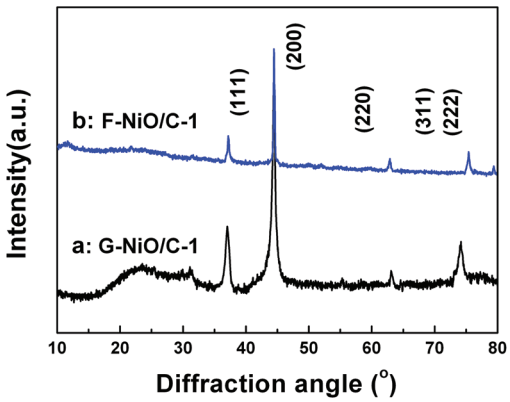

Fig. 1 X-ray diffraction pattern of G-NiO@C-1 and F-NiO@C-1.

Fig. 1 displays the X-ray diffraction (XRD) pattern of samples with high NiO contents. For example, the product XRD patterns of F-NiO@C-1 and G-NiO@C-1 show clearly peaks at 37.3°, 43.4°, 63.0°, 75.5° and 79.5°. These intense lines can be indexed to the (111), (200), (220), (311) and (222) planes of NiO with face-centered cubic structure which agrees well with the reported data (JCPDS card no. 65-29019). The relatively broadened peaks display NiO crystals of small size. The wide diffraction about 25.0° can be attributed to amorphous carbon frameworks. It has been reported that the carbon-rich phenolic resin can be carbonized at a temperature above 400 °C.[22,28] Therefore, the composites are composed of NiO nanoparticles and lignin-derived carbons.

Detailed structural information on the NiO@MPC was analyzed using TEM at different magnifications. From a low magnification TEM image (Fig. 2a–c), it is clear that the monodispersed nanoparticles with around 20 nm diameter are uniformly encapsulated in the mesoporous carbon. Particle aggregation on the wall of the carbon mesostructure can be excluded, indicating a restriction of phase separation between the NiO and the carbon framework upon heating. The disordered mesoporous feature of carbon can be confirmed by high magnification TEM images (Fig. 2d and e, the bright holes). Distinct lattice spacings with an interplanar distance of 0.21 nm are observed (Fig. 2f), corresponding to the spacing of the (200) planes of NiO crystals. These observations are in good agreement with the XRD results. The size of NiO nanoparticles will enlarge by increasing the feed ratio of Ni/C (shown in Fig. S2†), which has negative effects on supercapacitors.[29] The composition of the products is further examined by EDX (Fig. S1†). There are C, O, Ni, Cu and S peaks in the spectrum. The S element was the residue of lignosulfonate after the calcination. No other impurities were detected.

In order to determine the content of carbon, a TG analysis was used under an oxygen atmosphere for NiO@MPCs (shown in Fig. 3). For samples of G-NiO@C-1 and F-NiO@C-1, the results show that the weight losses are about 51.2% and 49.5%

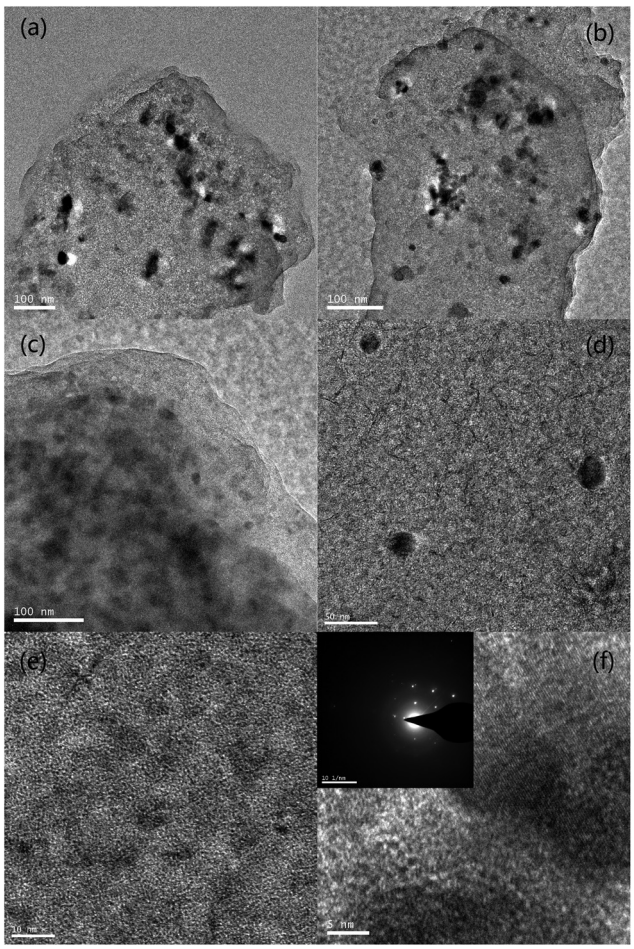

Fig. 2 TEM images of resulting NiO@MPCs: (a) G-NiO@C-1; (b) F-NiO@C-1; (c) G-NiO@C-3; (d) higher magnification of G-NiO@C-3; (d) observation of mesopores of G-NiO@C-3; (e) lattice spacings and Debye rings of NiO nanoparticles.

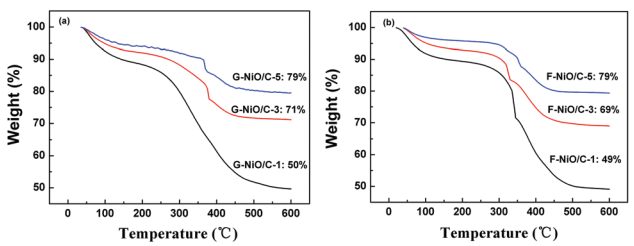

Fig. 3 TG curves of resulting NiO@MPCs: (a) G-NiO@C-*x*; (b) F-NiO@C-*x*.

between 230 and 600 °C, respectively, which is due to the carbonization of carbon. As summarized in Table 1, when increasing the feed ratio of Ni/C, the residual weight is higher than 79.2 wt%. So the content of carbon in NiO@MPCs is varied in a range of 20.8 wt% to 51.2 wt%.

Nitrogen adsorption and desorption isotherms and the pore size distribution curves are shown in Fig. 4. Typical type-IV nitrogen sorption isotherms with H2-type hysteresis loops in the range of *ca.* 0.45–1.0 P/P_0 were obtained for all of the NiO@MPCs, suggesting the existence of imperfect cylindrical

Table 1 The pore structural parameters of resulting NiO@MPC materials

Sample	NiO content[a] (wt%)	S_{BET}[b] ($m^2\ g^{-1}$)	V_{total}[c] ($cm^3\ g^{-1}$)	V_m[d] ($cm^3\ g^{-1}$)	D_p[e] (nm)	Peak value[f] (nm)
Pure carbon	0.0	685	0.436	0.208	3.7	3.7
G-Ni@C-1	50.3	622	0.476	0.020	3.6	3.6, 9.8
G-Ni@C-3	70.6	802	0.680	0.050	3.7	3.7, 9.7
G-Ni@C-5	79.2	716	0.487	0.009	3.7	3.6, 9.7
F-Ni@C-1	51.3	704	0.593	0.007	3.6	3.6
F-Ni@C-3	69.8	759	0.622	0.014	3.7	3.7
F-Ni@C-5	79.1	603	0.469	0.012	3.7	3.7

[a] Determined by TG analysis. [b] Calculated by the BET method using adsorption data in the P/P_0 range from 0.05 to 0.25. [c] Estimated from the adsorbed amount at P/P_0 = 0.995. [d] Calculated by the *t*-plot method. [e] Derived from the adsorption branches of the isotherms by the BJH method. [f] Derived from the peak value of pore size distribution.

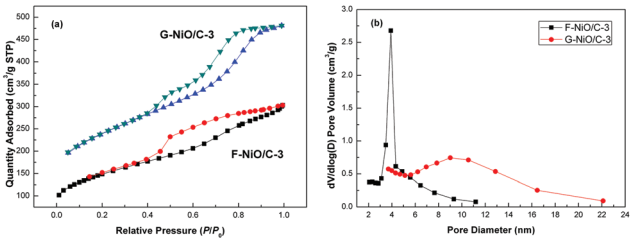

Fig. 4 (a) N_2 adsorption–desorption isotherms and (b) pore size distribution curves of representative G-NiO@C-3 and F-NiO@C-3 samples.

channels of uniform size. The calculated BET surface areas, pore volumes, and pore sizes are shown in Table 1. This series of materials is characterized by high surface areas (503–802 $m^2\ g^{-1}$), uniform pore sizes (≈3.7 nm), and large pore volumes (0.46–0.68 $cm^3\ g^{-1}$). These results reflect the fact that the uniform mesopores are opened with removal of the triblock copolymer after heating. Interestingly, the materials using glutaraldehyde as a CLA (labelled G-Ni@C-X) show a double-peak mesostructure, which is dispersed at 3.6 nm and 9.2 nm. In comparison, the materials using formaldehyde as a CLA (labelled F-Ni@C-X) show only one mesoporous distribution at 3.7 nm. Considering the molecular difference between formaldehyde and glutaraldehyde, it is believed that the long carbon chain of the glutaraldehyde structure caused a laxer assembly with the LC phase, resulting in larger BET surface area and double peaks of unique pore size distribution. From the data, we may see some slit-like pores except the main cylindrical pores, and as these are not the main contributions to the total volume, we referred to them as cylindrical pores for convenience. Matos *et al.* used sodium silicate and triblock copolymer template synthesized large-pore silica with a cage-like structure. They deemed that the size of these framework pores may extend beyond the micropore range and the framework pores and perhaps some of the pores connecting the mesopore can also be referred to as mesopores.[30,31] This phenomenon may influence the electrochemical properties of resulting NiO@MPC materials. It is reckoned

that the NiO@MPC, with the unique structures of high BET surface area and uniform mesoporous size, will provide the possibility of efficient transport of electrons and ions in electrodes, hence leading to high electrochemical performance. In comparison, a pure carbon sample was synthesized by the same method, and a similar mesoporous structure can be confirmed (shown in Fig. S4†), indicating that the lignin can be easily employed in the MPC.

The electrochemical properties of NiO@MPCs were measured using a three-electrode cell system. Standard cyclic voltammetry (CV) and galvanostatic charge–discharge techniques were used to test the electrochemical properties. The CV curves of the NiO@MPC composites (Fig. 5a and 6b) imply that the capacitance of the material is mainly associated with

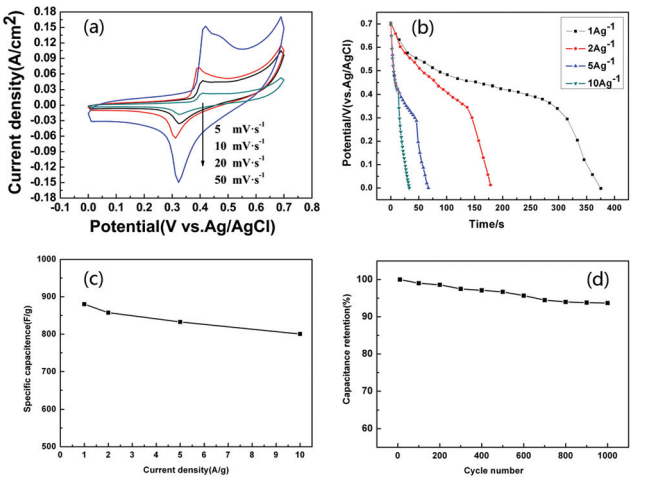

Fig. 5 Electrochemical measurements of a representative G-NiO@C-3 electrode investigated in 6 M KOH solution: (a) CV curves at different scan rates; (b) discharge curves of NiO@MPC at different current densities; (c) specific capacitance as a function of current; (d) charge–discharge cycle test.

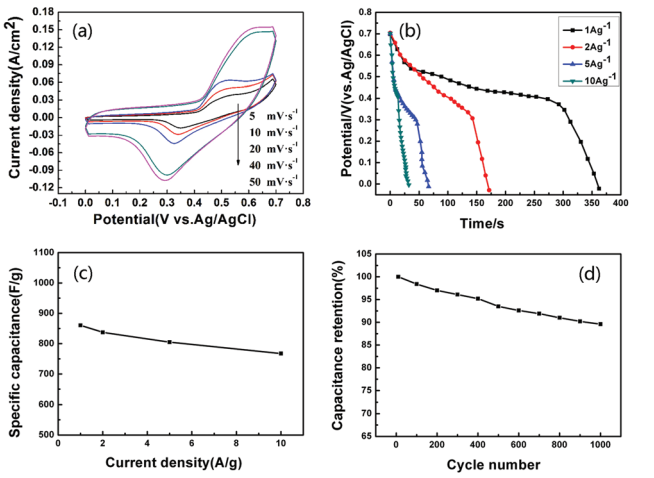

Fig. 6 Electrochemical measurements of a representative F-NiO@C-3 electrode investigated in 6 M KOH solution: (a) CV curves at different scan rates; (b) discharge curves of NiO@MPC at different current densities; (c) specific capacitance as a function of current; (d) charge–discharge cycle test.

the Faradaic pseudo-capacitor based on a fast redox mechanism and the transfer of the electron is reversible.[32] It is noted that the redox process of the G-NiO@C-3 electrode is more obvious than that of the F-NiO@C-3 electrode. The anodic peak at roughly 0.57 V is due to the oxidation of NiO to NiOOH, and the cathodic peak at about 0.29 V is for the reverse process. These peaks correspond to the conversion between different oxidation states of NiO according to the following eqn (2):

$$NiO + OH^- \leftrightarrow NiOOH + e^- \quad (2)$$

When the scan rate increases, the shape of the CV curves does not change noticeably (shown in Fig. 5a and 6a). This shows that the electrode material has very high electrochemical reactivity and fast activation indicating high electrical conductivity. With the increase of scan rates, the potentials of both peaks shift to more positive and negative directions. This may be attributed to the strengthened electric polarization and irreversible reactions at a higher scan rate. Because the reaction is limited by the ion diffusion rate, it is not going to satisfy electronic neutralization during the redox reaction.[33] Compared with G-NiO@C-3 (Fig. S3a†), the F-NiO@C-3 material shows a similar redox reaction (Fig. S3b†). It is confirmed that the mesoporous carbon has accelerated the electron transfer rate.

Furthermore, charge–discharge experiments were used to test the ability for capacitors. The relationship between specific capacitance and current density was also investigated. Fig. 5b shows the results gained for the G-NiO@MPC-3 electrode in the potential range of 0–0.7 V in 6 M KOH at various current rates (1.0, 2.0, 5.0 and 10.0 A g^{-1}). In this way, the specific capacitances of the NiO materials at 1.0, 2.0, 5.0 and 10.0 A g^{-1} were 880.2, 857.5, 832.7 and 800.5 F g^{-1}, respectively. Recently, Song *et al.* reported that bare NiO with a hollow and mesoporous structure has a specific capacitance of 770 F g^{-1} at a current density of 2 A g^{-1}.[34] The results indicate that the encapsulated MPC structure increases the specific capacitance of NiO more greatly than bulk NiO crystals (see Table S1†). The shape of the discharge curves is different from the double-layer capacitor, which was shown to be linear, implying its pseudo-capacitance nature. This is in good agreement with the result of the CV curves. The decrease in specific capacitance on increasing the discharge current is similar to the trend of capacitance variation from the CV studies. The F-NiO@C-3 electrode also has excellent specific capacitance as shown in Fig. 6b. The specific capacitances of the NiO@MPC material at 1.0, 2.0, 5.0 and 10.0 A g^{-1} were 860.4, 837.3, 804.9 and 767.5 F g^{-1}, respectively. Compared with that of G-NiO@C-3, a slightly smaller specific capacitance was obtained. The detailed specific capacitances of NiO@MPCs are tabulated in Table 2. It is noted that the NiO@MPC sample containing 79 wt% NiO shows less specific capacitance than the sample containing 70 wt% NiO, indicating that the surface area of NiO@MPCs and the size of NiO nanoparticles are important for electron transfer.

The rate capability is another important factor required for practical applications. For G-NiO@C-3 and F-NiO@C-3 electrodes (Fig. 5c and 6c), 90.9% and 89.2% of capacitances are retained

Table 2 Calculated specific capacitances of NiO@MPC composites at different discharge current densities

Current density (A g^{-1})	C_s[a] (F g^{-1})					
	G-NiO@C-1	G-NiO@C-3	G-NiO@C-5	F-NiO@C-1	F-NiO@C-3	F-NiO@C-5
1	705.1	880.2	802.6	645.8	860.4	776.3
2	685.0	857.5	782.5	622.4	837.3	756.7
5	660.8	832.7	755.0	595.1	804.9	735.2
10	624.9	800.5	722.8	565.7	767.5	706.9

[a] Calculated from the galvanostatic constant-current charge–discharge test.

when the current density changes from 1 A g^{-1} to 10 A g^{-1}, respectively. Compared to pure carbon and NiO compounds (see Table S1†), whose stabilities are not good and electrical properties perform poorly, the composites show terrific electrode properties. Jin *et al.* reported that a carbon material from high ash biochar has a specific capacitance of 260 F g^{-1} at a current density of 0.6 A g^{-1} and Fan *et al.* synthesized a biomass-derived porous carbon foam material that has a specific capacitance of 336 F g^{-1}.[35,36] The excellent rate capability is mainly attributed to the following two reasons: first, the NiO@MPC provides a large specific surface area for electrolyte access and shortens the diffusion path in the solid phase, resulting in fast redox reactions; second, the mesoporous structure has good stability and cannot easily collapse.[37]

Furthermore, the cyclability test confirmed the advances of NiO@MPC materials applied in supercapacitors. Fig. 5d and 6d show the specific capacitance variation for G-NiO@C-3 and F-NiO@C-3 as a function of cycle number at a current density of 1.0 A g^{-1} within a voltage range between 0 and 0.7 V. There are only 7.3% and 10.4% specific capacitance losses for the G-NiO@C-3 and F-NiO@C-3 electrodes after 1000 cycles, respectively, revealing the good stability of the product. The NiO@MPC using glutaraldehyde as a CLA exhibits more enhanced electrochemical properties. It is demonstrated that this mesoporous structure is beneficial to the diffusion of OH ions and the active site accessibility during the cycling process. The carbon layer coated on the surface of the NiO nanoparticles overcomes the poor conductivity of metal oxide. Moreover, the outer mesoporous carbon shells not only construct the conducting pathway for the system's electron transfer but also prevent the inner nanoparticles from aggregation and pulverization. The mesoporous feature of the carbon shell not only ensures interaction between the electrolyte and the active inner materials, but also digests the possible volume changes during cycling.

Conclusions

NiO-containing mesoporous carbon materials have been successfully synthesized by the LC phase-templating approach. Lignin, a biowaste and by-product from the paper industry, is polymerized with formaldehyde or glutaraldehyde used as a carbon precursor. The Ni-based intermediate obtained from the self-assembly in the carbon framework can be simply converted into highly crystalline NiO nanoparticles, which are covered by mesoporous carbon derived from cross-linked lignin polymers. As predicted, the resulting NiO@MPC, when applied as a supercapacitor electrode, exhibited a higher specific capacitance of 880.2 F g^{-1} at a current density of 1.0 A g^{-1} with enhanced rate capability and cycle stability. Such excellent capacitive behaviors are attributed to the unique mesoporous structures. The findings in the present work are important not only for the synthesis of the mesoporous carbon using lignin biomass, but also for the development of advanced electrode materials based on transition metal oxides for the enhancement of capacitive performance. This special structure may have other important applications, such as catalysis, sensors, and so on.

Acknowledgements

This material is based upon work funded by the Natural Science Foundation of China under grant nos. 21274131, 51273178 and 51203139. This work is also supported by the Natural Science Foundation of Zhejiang Province (LY12E03004 and LQ12E03004) and the Science and Technology Innovative Research Team of Zhejiang Province (no. 2009R50010).

Notes and references

1 M. Winter and R. J. Brodd, *Chem. Rev.*, 2004, **104**, 4245.
2 Y. G. Guo, J. S. Hu and L. J. Wan, *Adv. Mater.*, 2008, **20**, 2878.
3 Y. Meng, D. Gu and F. Q. Zhang, *J. Mater. Chem.*, 2006, **18**, 4447.
4 X. Wang, A. Yuan and Y. Wang, *J. Power Sources*, 2007, **172**, 1007.
5 P. Simon and Y. Gogotsi, *Nat. Mater.*, 2008, **7**, 845.
6 J. R. Miller and P. Simon, *Science*, 2008, **321**, 651.
7 J. J. Xu, K. Wang, S. Z. Zu, B. H. Han and Z. X. Wei, *ACS Nano*, 2010, **4**, 5019.
8 R. B. Moghaddam and P. G. Pickup, *Phys. Chem. Chem. Phys.*, 2010, **12**, 4733.
9 T. Nathan, A. Aziz, A. F. Noor and S. R. S. Prabaharan, *J. Solid State Electrochem.*, 2008, **12**, 1003.
10 J. P. Liu, J. Jiang, M. Bosmanc and H. J. Fan, *J. Mater. Chem.*, 2012, **22**, 2419.
11 H. Zhang, G. P. Cao, Z. Y. Wang, Y. S. Yang, Z. J. Shi and Z. N. Gu, *Nano Lett.*, 2008, **8**, 2664.
12 C. Z. Yuan, B. Gao, L. F. Shen, S. D. Yang, L. Hao, X. J. Lu, F. Zhang, L. J. Zhang and X. G. Zhang, *Nanoscale*, 2011, **3**, 529.
13 H. Jiang, L. P. Yang, C. Z. Li, C. Y. Yan, P. S. Lee and J. Ma, *Energy Environ. Sci.*, 2011, **4**, 1813.
14 X. R. Wang, S. M. Tabakman and H. J. Dai, *J. Am. Chem. Soc.*, 2008, **130**, 8152.

15 H. T. Zhang, X. Zhang, D. Zhang, X. Z. Sun, H. Lin, C. H. Wang and Y. W. Ma, *J. Phys. Chem. B*, 2013, **117**, 1616.
16 H. Jiang, T. Sun, C. Li and J. Ma, *RSC Adv.*, 2011, **1**, 954.
17 W. Wang, H. Y. Wang, W. Wei, Z. G. Xiao and Y. Wan, *Chem.–Eur. J.*, 2011, **17**, 13461.
18 C. Yu, B. Tian and D. Zhao, *Curr. Opin. Solid State Mater.*, 2003, **7**, 191.
19 S. A. El-Safty, T. Hanaoka and F. Mizukami, *Chem. Mater.*, 2005, **17**, 3137.
20 Y. H. Deng, T. Yu, Y. Wan, Y. F. Shi, Y. Meng, D. Gu, L. J. Zhang, Y. Huang, C. Liu, X. J. Wu and D. Y. Zhao, *J. Am. Chem. Soc.*, 2007, **129**, 1690.
21 Y. Huang, H. Q. Cai, T. Yu, F. Q. Zhang, F. Zhang, Y. Meng, D. Gu, Y. Wan, X. L. Sun, B. Tu and D. Y. Zhao, *Angew. Chem., Int. Ed.*, 2007, **46**, 1089.
22 F. Zhang, D. Gu, T. Yu, F. Zhang, S. Xie, L. Zhang, Y. Deng, Y. Wan, B. Tu and D. Zhao, *J. Am. Chem. Soc.*, 2007, **129**, 7746.
23 Y. Zhai, Y. Dou, D. Zhao, P. F. Fulvio, R. T. Mayes and S. Dai, *Adv. Mater.*, 2011, **23**, 4828.
24 F. S. Chakar and A. J. Ragauskas, *Ind. Crops Prod.*, 2004, **20**, 131.
25 J. L. Braun, K. M. Holtman and J. F. Kadla, *Carbon*, 2005, **43**, 385.
26 X. P. Dong, W. H. Shen, J. L. Gu, L. M. Xiong, Y. F. Zhu, H. Li and J. L. Shi, *J. Phys. Chem. B*, 2006, **110**, 6015.
27 J. Horiguchi, Y. Kobayashi, S. Kobayashi, Y. Yamazaki, K. Omata, D. Nagao, M. Konno and M. Yamada, *Appl. Catal., A*, 2011, **392**, 86.
28 C. D. Liang and S. Dai, *J. Am. Chem. Soc.*, 2006, **128**, 5316.
29 M. Kruk, M. Jaroniec, C. H. Ko and R. Ryoo, *Chem. Mater.*, 2000, **12**, 1961.
30 J. R. Matos, L. P. Mercuri, M. Kruk and M. Jaroniec, *Langmuir*, 2002, **18**, 884.
31 J. W. Lang, L. B. Kong, W. J. Wu, Y. C. Luo and L. Kang, *Chem. Commun.*, 2008, 4213.
32 S. B. Yang, X. L. Wu, C. L. Chen, H. L. Dong, W. P. Hu and X. K. Wang, *Chem. Commun.*, 2012, **48**, 2773.
33 L. Fan, L. Tang, H. Gong, Z. Yao and R. Guo, *J. Mater. Chem.*, 2012, **22**, 16376.
34 C. Y. Cao, W. Guo, Z. M. Cui, W. G. Song and W. Cai, *J. Mater. Chem.*, 2011, **21**, 3204.
35 H. Jin, X. M. Wang, Z. R. Gu and J. Polin, *J. Power Sources*, 2013, **236**, 285.
36 Z. J. Fan, D. P. Qi, Y. Xiao, J. Yan and T. Wei, *Mater. Lett.*, 2013, **101**, 29.
37 Y. Q. Zhang, X. H. Xia, J. P. Tu, Y. J. Mai, S. J. Shi, X. L. Wang and C. D. Gu, *J. Power Sources*, 2012, **199**, 413.